Tuning the magnetic properties of V₂O₃/CoFeB heterostructures across the V₂O₃ structural transition

V. Polewczyk [1,*] S. K. Chaluvadi [1] P. Orgiani [1,2] G. Panaccione [1] G. Vinai [1] G. Rossi [1,3] and P. Torelli [1]

[1]*Istituto Officina dei Materiali (IOM)–CNR, Laboratorio TASC, Area Science Park, S.S.14, km 163.5, I-34149 Trieste, Italy*
[2]*CNR-SPIN, UOS Salerno, 84084 Fisciano, Italy*
[3]*Dipartimento di Fisica, Università degli Studi di Milano, Via Celoria 16, I-20133 Milano, Italy*

In this work, we investigate the effects of the V_2O_3 structural phase transition on the magnetic properties of an amorphous magnetic thin film of CoFeB in contact with it. V_2O_3 thin films are deposited epitaxially on sapphire substrates, reaching bulklike properties after few nm of growth. By means of temperature dependent Kerr effect characterizations, we prove that crossing the V_2O_3 structural phase transition induces reproducible and reversible changes to CoFeB magnetic properties, especially to its coercive field. By decreasing the oxide layer thickness, its effects on the magnetic layer decreases, while reducing the magnetic layer thickness maximizes it, with a maximum of 330% coercive field variation found between the two V_2O_3 structural phases. By simply tuning the temperature, this systematic study shows that the engineering of V_2O_3 structural transition induces large interfacial strain and thus strong magnetic property variations to an amorphous thin film, opening wide possibilities in implementing strain-driven control of the magnetic behavior without strict requirements on epitaxial coherence at the interface.

I. INTRODUCTION

In the last decades, many attempts have been performed to find efficient and fast manipulation of magnetization in different material arrangements with the goal of reducing both the power required and the noise typical of *H*-field switching; the use of electric fields [1,2], light [3,4], acoustic waves [5–7], injection of spin-polarized currents [8–10], morphology [11–13], or strains are pursued to reach this goal. Indeed, the latter is now commonly used to tailor material properties by modifying the crystalline structure and/or the electron-lattice interactions [14]. Recent results on the enhancement/creation of ferroelectric polarization [15,16], tailoring of the Curie temperature [17,18], and superconductivity critical temperature [19] have been reported.

Strain can be introduced in the active magnetic layers by different mechanisms: (i) purely mechanical strain [20,21], (ii) application of electric fields in ferro/piezoelectric materials [22], (iii) optical photostriction [23], (iv) structural phase transitions (SPTs) [24,25].

Vanadium sesquioxide (V_2O_3) is a highly correlated oxide particularly attractive in this research because of its first-order phase transition around 160 K from a rhombohedral paramagnetic high temperature metallic state to a monoclinic antiferromagnetic low-temperature insulating state [26,27], therefore combining a metal-insulator transition (MIT) to a SPT one [24]. The associated volume expansion is of 1.4% when going from the high-temperature phase to the low-temperature one [28]. Bulk V_2O_3 undergoes a destructive MIT

due to the large volume increase, which can result in the single crystal sample turning to powder [29]. For this reason, several studies have been focused on the nondestructive MIT of V_2O_3 thin films [30–33], which display bulklike properties at thicknesses of a few nm [34] while undergoing nondestructive and reversible SPTs, as evidenced by temperature dependent x-ray diffraction characterizations [35–37]. These thin films can be exploited as elements of hybrid magnetic heterostructures therefore offering unique opportunities for the design of functional material systems [33,38–40]. However, up to now, few studies have concentrated on the interfacial coupling as a function of the thickness of both the oxide and the magnetic layers [33,40].

We present here a systematic study on the strain-driven changes on the magnetic properties of $V_2O_3/Co_{60}Fe_{20}B_{20}$ (CoFeB) heterostructures, thus including one of the most widely used materials in spintronics, from magnetic tunnel junctions [41,42] to spin-transfer torque [43], spin pumping [44] or spin Hall effect [45]–based devices. With a magnetostriction coefficient comparable to those of other transition metals such as Co [46], and very small anisotropy [47] and low coercivity, it is expected to be sensitive to the effects of the SPT at the interface. V_2O_3 thin films of thicknesses in the 5–80-nm range were grown in UHV by pulsed laser ablation deposition (PLD) on sapphire and their structural and electrical properties were characterized. We subsequently grew on top of the atomically clean surface different thicknesses of CoFeB, by physical vapor deposition in UHV, and studied their magnetic properties as a function of temperature [48]. In the temperature range above the V_2O_3 MIT transition the magnetic coercive field (H_C) of CoFeB has a negligible temperature dependence, but a sharp increase of H_C is

*polewczyk@iom.cnr.it
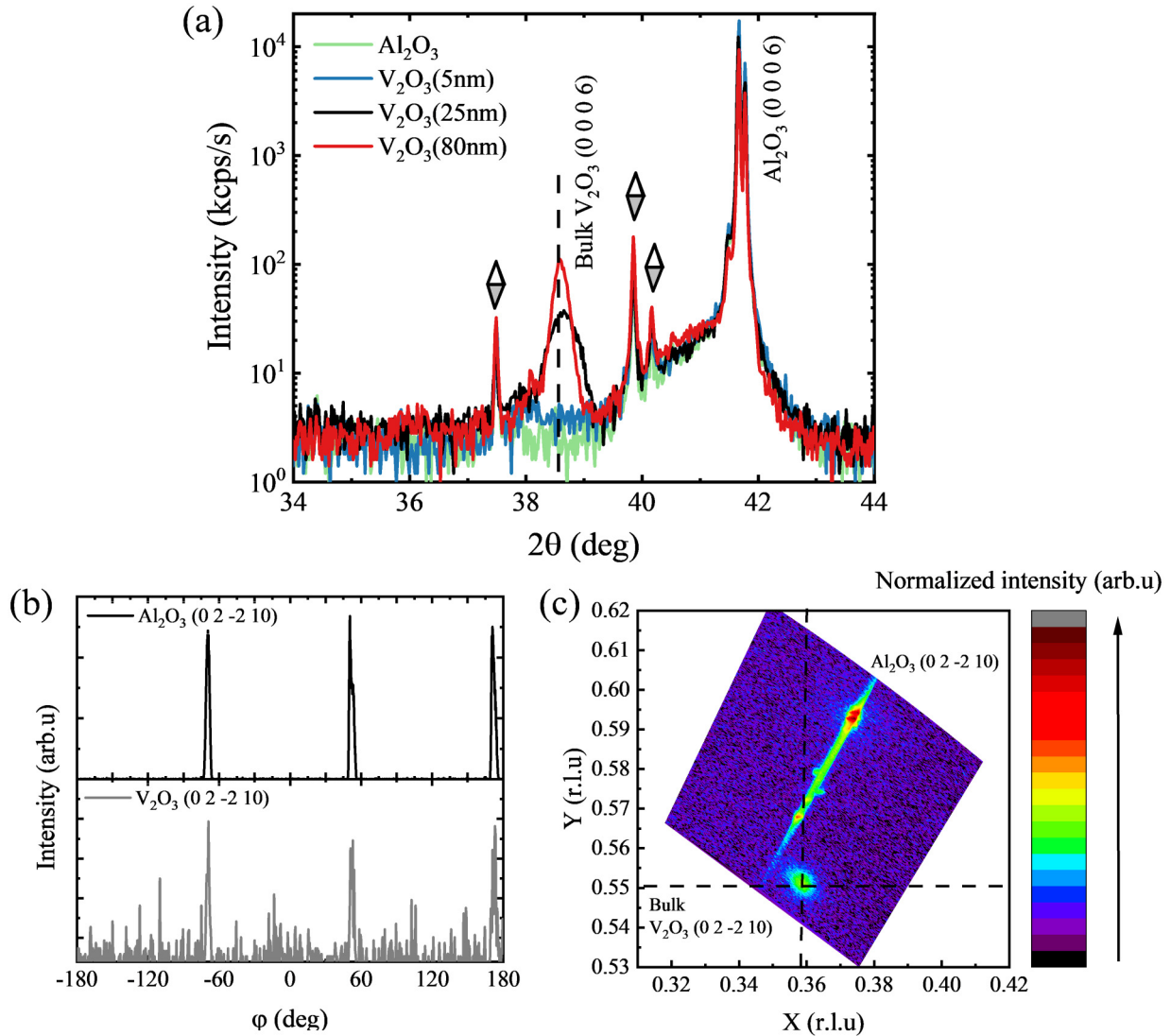
FIG. 1. (a) θ-2θ scans recorded on Al_2O_3/$V_2O_3(t)$/CoFeB(30 nm)/MgO for different oxide thicknesses: 0 nm (green), 5 nm (blue), 25 nm (black), and 80 nm (red). Diamonds indicate the spurious diffraction peaks coming from the nonmonochromatic source. For the 25-nm-thick V_2O_3 (b), φ scans are shown on the (0 2 −2 10) reflection of the substrate (black) and the oxide (grey) as well as (c) normalized 2D reciprocal space map around this reflection. In (a) and (c), the bulk values of V_2O_3 are pointed out by a dashed line.

observed after crossing the phase transition reaching a maximum coercive field change of 330% between room temperature (RT) and 77 K [from now on, low temperature (LT)] for the heterostructure made of $V_2O_3(80 \text{ nm})$/CoFeB(3 nm), i.e., a thick oxide layer and very thin CoFeB. While decreasing the V_2O_3 layer thickness reduces the effect of the SPT on the coercive field of CoFeB; the highest sensitivity to the SPT of the substrate oxide is obtained for the thinnest magnetic layer. Our results show how tuning the thicknesses of both layers in the heterostructure can tailor the strain-induced effects on the magnetic properties. V_2O_3 appears clearly as a promising candidate for functional strain-driven magnetic heterostructures. Moreover, a similar study could be now extended to other compounds belonging to the same family, such as, for example VO_2, which presents a structural phase transition just above room temperature [49].

II. EXPERIMENTAL DETAILS

Highly (0 0 0 1)-oriented *c*-plane sapphire substrates were cleaned with acetone and ethanol in an ultrasonic bath, and outgassed in air at 400 K for 30 min before being introduced in the ultra high vaccum (UHV) deposition and characterization apparatus.

Epitaxial V_2O_3 (0 0 0 1) thin films of different thicknesses were deposited on the substrate by PLD technique using a Nd:YAG laser of 1064 nm wavelength (first harmonic, as described in [50]) and a laser repetition rate of 1 Hz, leading to a deposition rate of 13 Å min^{-1}, with thicknesses in the range from 5 to 80 nm. The films were deposited at a pressure lower than 10^{-7} mbar, at a substrate temperature of 1000 K, with a substrate to target distance of 6 cm. After deposition, the films were cooled down to RT under UHV. We first characterized, *ex situ*, the film resistivity as a function of temperature

using the four-probe van der Pauw method. The oxide films were subsequently transferred into the UHV apparatus for the deposition of $Co_{60}Fe_{20}B_{20}$ by *e*-beam evaporation of a stoichiometric sample [48] without performing any preliminary chemical or physical surface treatment. CoFeB thin films of different thicknesses were deposited at a pressure never exceeding 1.10^{-9} mbar, with a deposition rate of 2 Å min^{-1} while maintaining the substrate at RT. Shadowing effects [51] were minimized by orienting the sample surface perpendicularly to the metal vapor beam average direction during the deposition. Together with these samples, Al_2O_3/CoFeB reference samples were grown under the same conditions. The angular and temperature dependent magnetic characterization of the V_2O_3/CoFeB samples was performed by *in situ* longitudinal magneto-optic Kerr effect (MOKE) measurements. Measurements were taken, ranging from RT to LT, using a *s*-polarized red laser (658 nm) and a photoelastic modulator (PEM) operating at 50 kHz coupled to a lock-in setup, with a laser spot size of about 500 μm^2.

Before removing the samples from UHV, a 3-nm-thick MgO capping layer was deposited by electron gun evaporator with a deposition rate of 2 Å min^{-1} at RT. Finally, the structure and thickness of these heterostructures were characterized by x-ray diffraction (XRD), doing a specular, azimuthal phi scan and two-dimensional (2D) reciprocal space map around asymmetric Bragg reflections, and low-angle x-ray reflection (XRR) techniques with a PanAnalytical X'Pert Pro diffractometer (Cu-K_α wavelength). The whole sample growth and characterizations were carried out at the NFFA facility in Trieste [48].

III. RESULTS AND DISCUSSION

In Fig. 1 we present the specular θ-2θ scans of the Al_2O_3/$V_2O_3(t)$/CoFeB(30 nm)/MgO(3 nm) samples for *t* in the 5–80-nm range [Fig. 1(a)], along with the φ scan [Fig. 1(b)] and the 2D map reciprocal space map [Fig. 1(c)] around the Al_2O_3/V_2O_3 (0 2 −2 10) reflection for the 25-nm-thick V_2O_3 sample.

In Fig. 1(a) we observe a V_2O_3 (0 0 0 1) peak appearing along the same crystallographic direction of the substrate for thicknesses equal or larger than 25 nm, giving a hexagonal surface symmetry [52]. The intensity and sharpness of the peak reveal a good crystalline quality, further improving for larger thicknesses. This is confirmed by the small full width at half maximum of rocking curve across the V_2O_3 (0 0 0 6) Bragg peak of approximately 0.3° recorded for both 25 and 80 nm thicknesses (not shown here). A small tensile (compressive) in-plane (out-of-plane) strain of about 0.1–0.2% (0.4%) with respect to the substrate was found [from Figs. 1(a) and 1(c)] and may be attributed to high temperature deposition and different thermal dilatation coefficients between the deposited film and the substrate [53], changes in stoichiometry (O vacancies and/or defects) [31], or to ion bombardment issues [54]. Nonetheless, we can consider both thicknesses as relaxed oxide layers. From Fig. 1(b), the asymmetrical reflections of both substrate and V_2O_3 layer show peaks every 120°, evidencing the [0 0 0 1] oriented hexagonal phase structures with the in-plane orientation relationships V_2O_3 [0 1 −1 0] ∥ Al_2O_3 [0 1 −1 0].
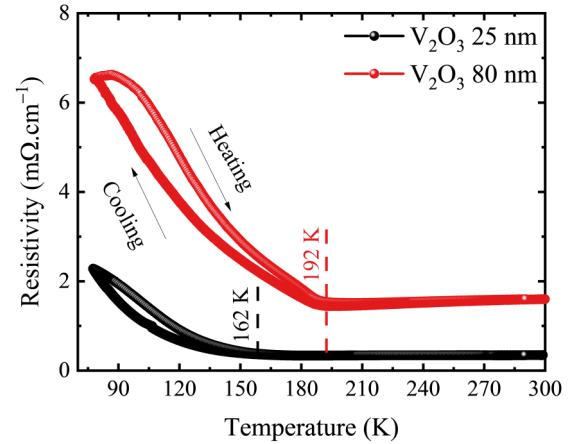
FIG. 2. Transport measurements collected between LT and RT for two different thickness of V_2O_3 thin films, 25 nm (black) and 80 nm (red). On both curves, the left branch corresponds to the cooling one and the right branch to the heating one.

Due to the large in-plane lattice mismatch of approximately 4% between the bulk V_2O_3 and the substrate, relaxation via introduction of misfit dislocations is expected to occur after a critical thickness of few nm [53]. To check it, the 2D reciprocal space map of Fig. 1(c) was recorded around the same (0 2 −2 10) reflection of both the Al_2O_3 substrate and V_2O_3 (25 nm). For both cases, the elliptical shape and broadening of the peak are due to the tilt of these diffracting planes and finite in- and out-of-plane coherence lengths. The peak position with respect to the substrate and its position and width in the *k* space prove that the film is relaxed, since its in-plane lattice parameter corresponds to the expected V_2O_3 bulk value of 0.49521 nm [52], as marked by the dashed lines in Fig. 1(c). Coherently with θ-2θ scans, this diffracted V_2O_3 plane started being detectable for thicknesses of 25 nm and similar results were obtained for the 80-nm-thick film. In all these experiments, no magnetic diffraction peaks were found, confirming their amorphous types.

Figure 2 shows the resistivity temperature dependence of two V_2O_3 thicknesses, 25 nm (black) and 80 nm (red), prior the CoFeB deposition. The characterization of the thinnest V_2O_3 film of 5 nm could not be obtained as its signal was below the sensitivity of our setup.

The measured resistivity values at RT are consistent with results reported in literature [30,34] and close to the bulk value of 0.5 mΩ cm^{-1} [28]. The fact that RT resistivity of metallic V_2O_3 decreases when reducing the thin film thickness is counterintuitive, but already highlighted in previous studies [24,55], and can be tentatively attributed to an increase of defects (O vacancies [31] or ion bombardment effects [54]) or to the higher density of dislocations [53] in thicker films. When lowering the temperature, one can observe a change of slope for both samples displayed in Fig. 2, which is more marked for thicker films, and the opening of the loop in correspondence to the MIT. The values of the two MITs, as determined from the first derivative of the transport curves, are marked with vertical dotted lines. The MIT of bulk V_2O_3 is at around 170 K. In the thin films grown on single crystal substrates it may vary in temperature depending on the deposition
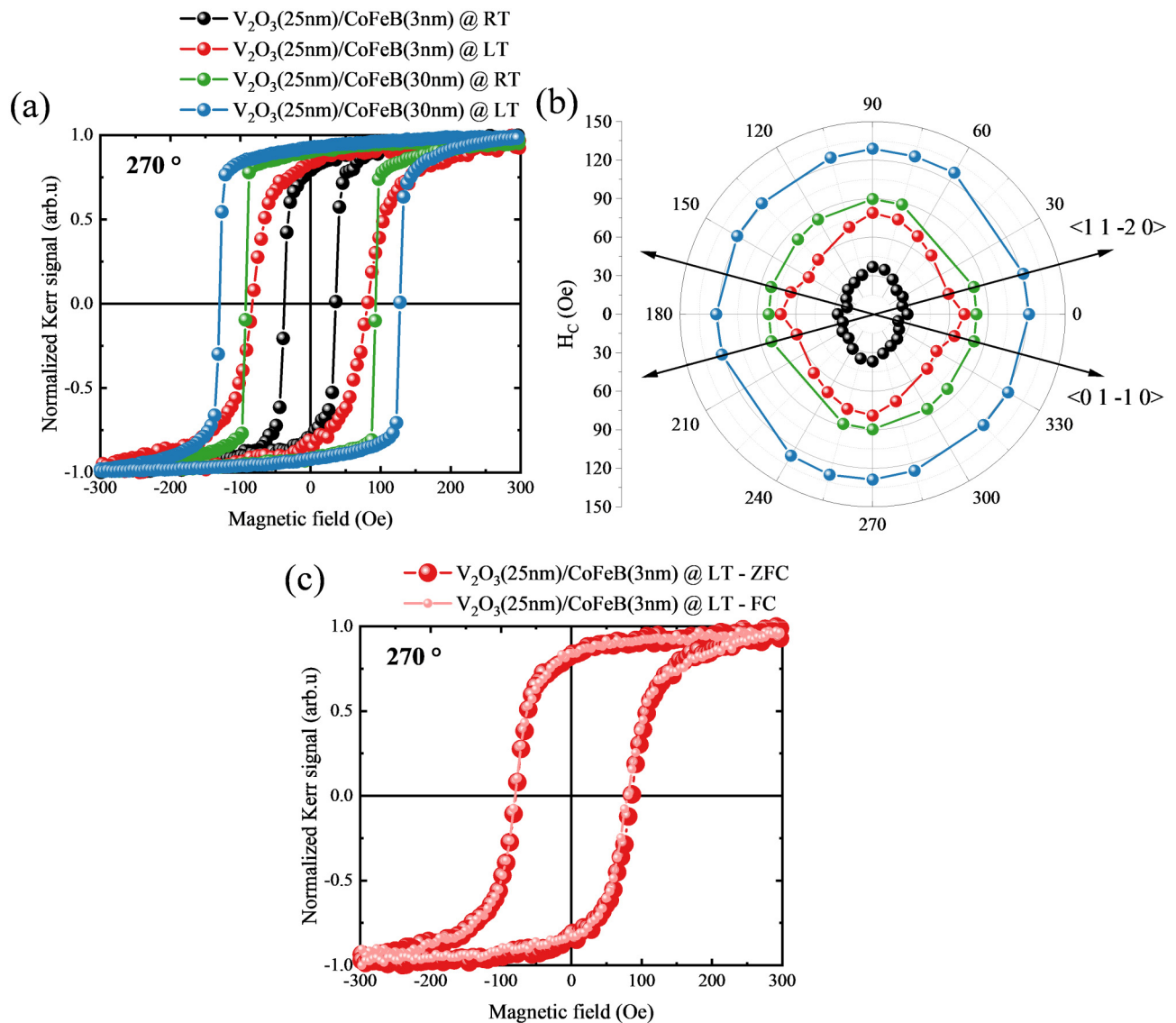
FIG. 3. (a) Hysteresis loops measured along 270° in-plane angle at two relevant temperatures, i.e., RT (black and green) and LT (red and blue), and for two different CoFeB thicknesses, i.e., 3 (black and red) and 30 nm (green and blue), deposited on 25-nm-thick V_2O_3. (b) Polar plot of the magnetic coercive field H_C measured for the same conditions. The two black arrows represent the in-plane crystallographic directions of both the substrate and V_2O_3. (c) Hysteresis loops of V_2O_3(25 nm)/CoFeB(3 nm) along the same angle are recorded at LT after ZFC (red) and FC (pink).

methods and conditions, such as pressure, temperature, and rate [31,34]. In particular, the MIT temperature is expected to increase with thickness, as already observed for unstrained films in [34]. Considering the resistivity curves below the MIT, the loop opening is quite similar for both film thicknesses, with a maximum of resistivity coercivity in temperature of approximately 10 and 20 K for 25 and 80 nm respectively. The origin of the hysteresis is due to the coexistence of insulating and metallic mesoscopic-nanoscopic domains crossing the MIT, whose working principle can be modeled as a percolative one [27]. The detailed analysis of the domain evolution and related kinetics are however beyond the scope of this work.

We explored the magnetic properties of the V_2O_3/CoFeB heterostructures by different methods; MOKE polar plots and temperature dependence were carried out for all combination

of V_2O_3 and CoFeB layer thicknesses. The reproducibility of all the following characterizations have been confirmed multiples times. Figure 3 shows (a) the in-plane hysteresis loops at a given angle and (b) the polar characterization of H_C for the two temperature limits (RT and LT) and for 3- and 30-nm-thick CoFeB deposited on 25-nm-thick V_2O_3. In addition, we compare the in-plane hysteresis loops after field cooling (FC) to LT under an in-plane magnetic field of 5000 Oe and after zero field cooling (ZFC), as depicted in Fig. 3(c).

The in-plane magnetic anisotropy for 3-nm-thick CoFeB is slightly uniaxial, with an easy axis of magnetization, identified by larger remanent magnetization and less rounded shape of the hysteresis loop, along the 90–270° axis, whose direction with respect to the crystallographic axis is shown in Fig. 3(b). Even if CoFeB is expected to be amorphous, multiple reasons can drive this small anisotropy, such as shadowing
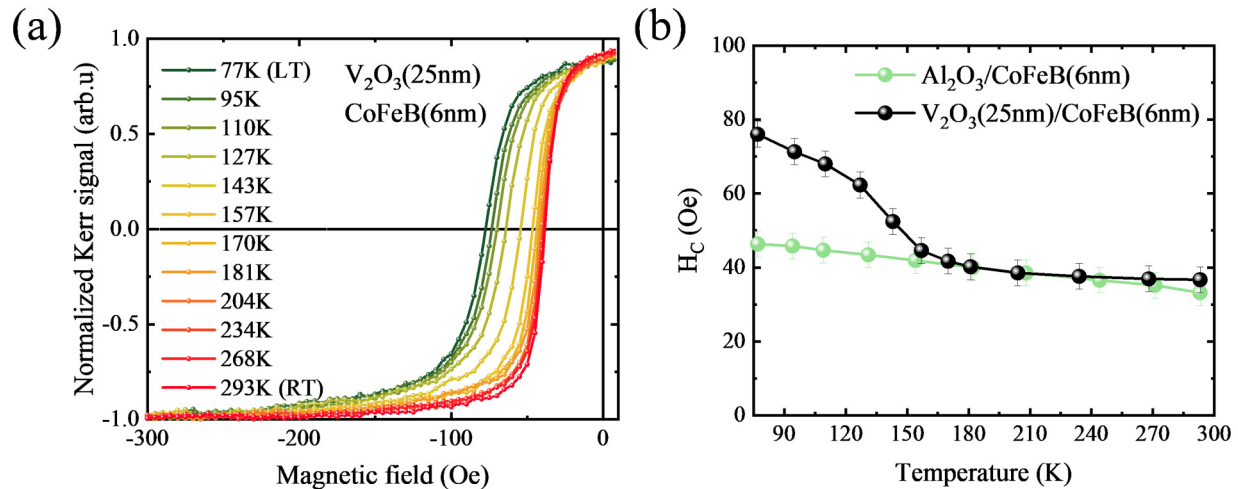
FIG. 4. (a) Half hysteresis loops of V_2O_3(25 nm)/CoFeB(6 nm) heterostructure along the easy between LT and RT. (b) H_C (T) curves for both the same (black) and the reference (green) samples.

effects [51], residual strains from the interface [56], or roughness [57]. Increasing the thickness of the CoFeB film leads to an increase of the coercive field values and to isotropic behavior with a larger remanent magnetization, suggesting the interfacial origin of the anisotropy present in the thinner films. The CoFeB thickness dependence of the coercive field has been observed previously [58,59], and it was explained by an increase of defects.

As expected from the Curie-Weiss law, for both CoFeB thicknesses, the coercive field increases at LT with the same anisotropic/isotropic (3 nm/30 nm) behavior observed at RT. Since the MIT of V_2O_3 is accompanied by a magnetic transition from paramagnetic at RT to antiferromagnetic at LT, we can infer that an additional interfacial magnetic effect of exchange bias coupling to the ferromagnetic layer. However, the magnetic hysteresis loops are identical [red and pink curves of Fig. 3(c)] after both FC and ZFC. Despite the formation of an antiferromagnetic/ferromagnetic interface at LT, no interfacial exchange bias field is measured, contrary to what is reported in the case of other V_2O_3/ferromagnetic heterostructures (Ni or Co) [40]. Such discrepancy, especially for small CoFeB thicknesses, may be due to the surface quality of the V_2O_3 after air exposure or to the relatively small setting field (5000 Oe) applied in our experiment and/or the formation of a dead layer, which was observed for Fe thin film on V_2O_3 [40]. Since no differences were observed, all the following H_C (T) curves were taken using ZFC treatment.

Temperature dependent hysteresis loops where then measured from LT up to RT (heating branch) by applying the magnetic field along the easy axis [90–270°] highlighted in Fig. 3(b) for the V_2O_3 (25 nm)/CoFeB(6 nm) sample and the Al_2O_3/CoFeB(6 nm) reference sample. Similar results were obtained along different in-plane axes (not shown). Figure 4(a) displays half of the hysteresis loops across the whole temperature range, while in Fig. 4(b) the correspondent values of coercive field are plotted and compared to those of the reference sample.

From the measurement in Fig. 4(a), one can see a sharp decrease of the coercive field from LT up to around 160 K,

i.e., in correspondence to the SPT, consistently with the resistivity measurements show in Fig. 2(b), while little changes in the hysteresis loops are measured above it, as displayed in Fig. 4(b). Moreover, the ratio between the magnetization at remanence and at saturation remains roughly constant over the whole temperature range without a marked variation when crossing the SPT temperature, as already observed in [33,36,39]. Here, the comparison between the reference sample and the heterostructure clearly shows the role of the SPT in the evolution of the V_2O_3/CoFeB coercive field. While the reference sample (in green) shows an almost constant, slight decrease of H_C when increasing the temperature, the V_2O_3/CoFeB heterostructure (black curve) clearly presents an additional contribution below the SPT, leading to an H_C value at LT whose magnitude is almost doubled. The V_2O_3 SPT volume expansion contributes to an additional strain/stress to the interfacial CoFeB layer compatible with an inverse magnetostrictive effect.

Before any tailoring of this strain-driven control of the magnetic behavior, we checked the reversibility of the observed trends by recording in Fig. 5 both heating (red) and
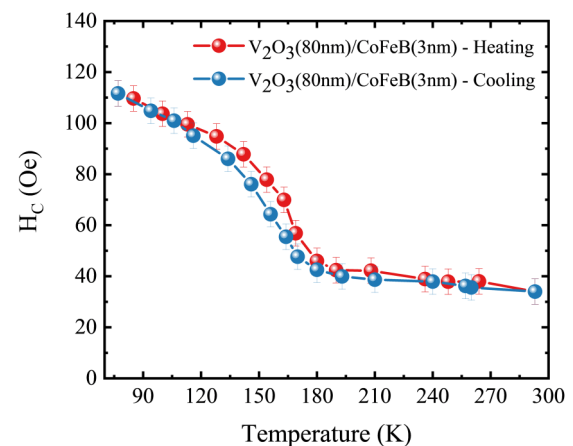
FIG. 5. H_C (T) curves of the V_2O_3(80 nm)/CoFeB(3 nm) heterostructure for both heating (red) and cooling (blue) branches.
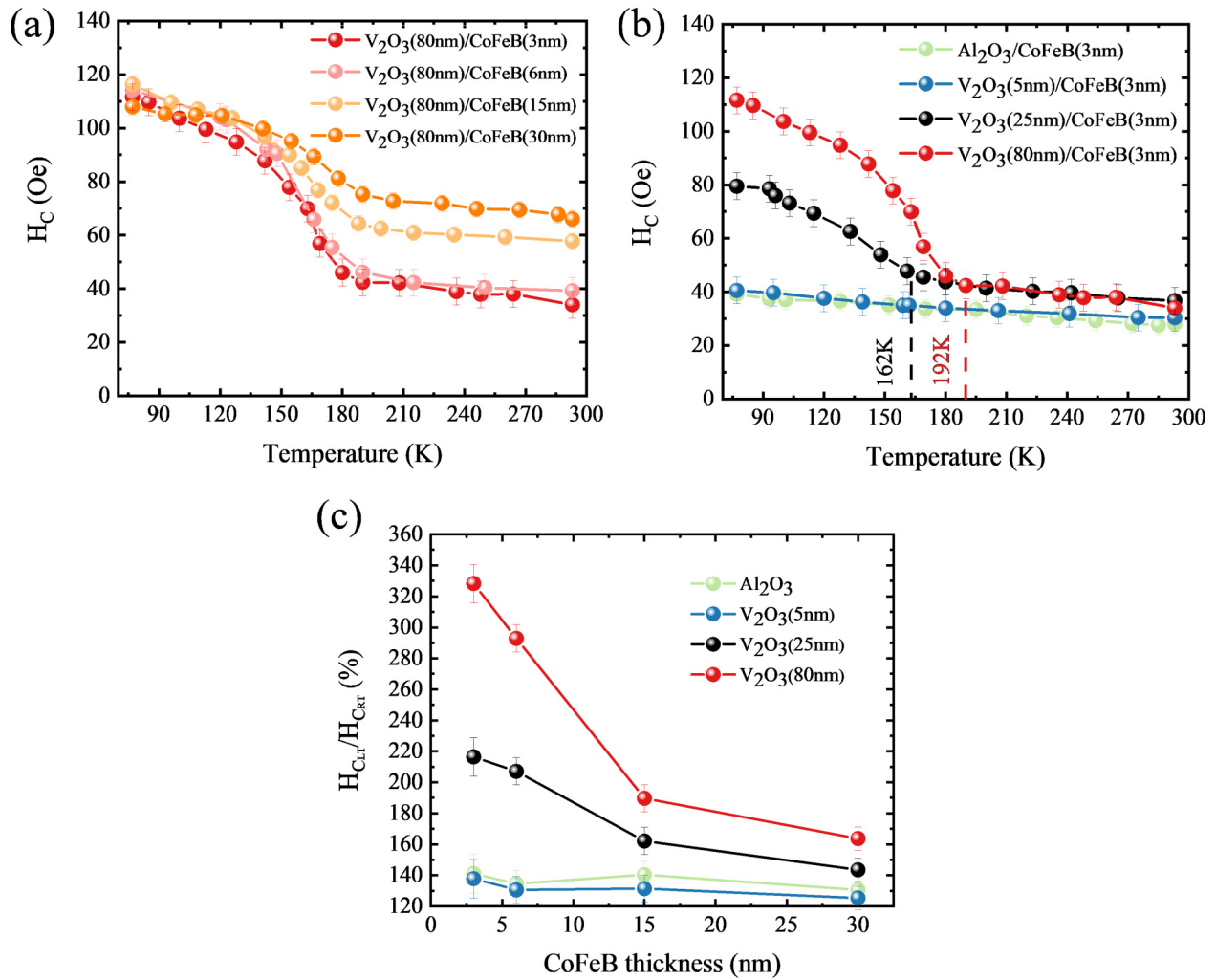
FIG. 6. (a) H_C (T) curves of the 80-nm-thick V_2O_3 for different CoFeB thicknesses: 3 nm (red), 6 nm (pink), 15 nm (light orange), and 30 nm (orange). (b) H_C (T) curves of the 3-nm-thick CoFeB for different V_2O_3 thicknesses, 0 nm (green), 5 nm (blue), 25 nm (black), and 80 nm (red). (c) Percentage variation of the coercive field measured between LT and RT for different thicknesses of V_2O_3 and CoFeB.

cooling (blue) branches for the V_2O_3(80 nm)/CoFeB(3 nm) heterostructure.

A small hysteresis in the coercive field variation appears in Fig. 5, which is consistent with the transport measurements shown in Fig. 1 and with findings reported for Ni heterostructures [27,33]. The change obtained in H_C is thus totally reversible between the two V_2O_3 structural phases, and it is especially evident at temperatures well below and above the SPT temperature. Therefore, all the subsequent H_C (T) curves were obtained by heating up the heterostructures. In addition to this important verification, we observed a larger coercive field variation for the V_2O_3(80 nm)/CoFeB(3 nm) sample with respect to that recorded in the case of the V_2O_3(25 nm)/CoFeB(6 nm) heterostructure shown in Fig. 4.

In Fig. 6, we show data that stress the role of the interfacial coupling by playing with the thicknesses of both layers in the heterostructure. First, by keeping the V_2O_3 thickness constant at 80 nm (i.e., the thickest case), the H_C temperature dependence of the whole range of CoFeB thicknesses is shown in Fig. 6(a). In Fig. 6(b), we fix the CoFeB thickness to 3 nm

(i.e., the lowest one) and explore the whole V_2O_3 thickness range. Finally, in Fig. 6(c) we sum up the coercive field variation between LT and RT, expressed in %, for the ensemble of samples.

Several conclusions can be drawn from the above results. As already observed in Figs. 3(a) and 3(b), the RT coercive field increases as a function of the CoFeB thickness [see Fig. 6(a)]. Interestingly, to this RT increase does not correspond a proportional increase of H_C at LT (below the SPT): the largest variation of H_C between RT and LT is measured for the thinnest CoFeB layers. On the other hand, when fixing the CoFeB thickness and changing the V_2O_3 thickness, the initial coercive field values measured at RT, as shown in Fig. 6(b), are quite similar among the different V_2O_3 thicknesses, and not far from those of the reference sample. Increasing the V_2O_3 thickness leads to higher SPT temperatures consistently with the transport data shown in Fig. 2.

If one compares Figs. 6(a) and 6(b), and as it is summarized in Fig. 6(c), the smaller the CoFeB thickness the larger the effect on the coercive field variation of the two V_2O_3 structural

phases: this clearly indicates that the observed effect is interface driven. On the other hand, the coupling effect decreases when reducing the V_2O_3 thickness till it disappears for 5 nm thickness: this can be attributed to the highly strained oxide layer whose SPT is likely to be inhibited. We observe a maximum coercive field variation of 330% between RT and LT for heterostructures between the thickest V_2O_3 substrate and the thinnest CoFeB ferromagnetic overlayer, corresponding to a coercivity variation of approximately 70 Oe. As mentioned in the introduction, the V_2O_3 oxide structure passes from rhombohedral to monoclinic, and experiences a three-dimensional volume expansion of 1.4% that influences both lattice and angle parameters [28], making the calculation of strain-induced changes in magnetization not trivial.

The coercive field temperature dependence of a relaxed ferromagnetic layer, i.e., in the absence of an induced temperature-dependent strain, has a linear behavior, as confirmed by the Al_2O_3/CoFeB case in Fig. 6(b), and expected from the standard Stoner-Wohlfarth model. The differences in the coercive field variations between a relaxed ferromagnetic layer and the V_2O_3/CoFeB case are directly linked to the strain variation induced by the SPT. In the presence of an external uniaxial stress, assumed to be uniform in a polycrystalline film, the additional magnetic anisotropy induced by the SPT of V_2O_3 is given by

$$H_k = \frac{3\lambda_s \sigma}{M_s},$$

where σ is the stress in MPa, λ_s is the saturation magnetostriction (-35 ppm in the case of $Co_{60}Fe_{20}B_{20}$ [46]), and M_s is the saturation magnetization (approximately $800\,\text{kA m}^{-3}$ in the case of $Co_{60}Fe_{20}B_{20}$ [46]). From the above equation, one can see that either an increase of λ_s or a decrease of M_S would increase the impact of the stress on the coercive field variation. This is coherent with the larger coercivity variations observed in the case of V_2O_3/Ni [33] compared to V_2O_3/Co [33,36,39].

The stress variation induced by V_2O_3 when crossing its SPT is expected to be constant all over the surface and roughly 550 MPa [33]. The additional coercive field induced by the stress is thus nearly 70 Oe, consistent with what obtained in the case of the thickest V_2O_3 substrate and thinnest

CoFeB ferromagnetic overlayer [see Figs. 6(b) and 6(c)]. Since stress/strain propagation is extremely sensitive to the interfacial roughness and microstructure [36], it is however not possible to easily model a more accurate quantitative comparison with other V_2O_3-based heterostructures with ferromagnetic materials such as Ni, Fe, or Co, where the order of magnitude of the strain-induced effects is comparable with what obtained in our case [33,36,39].

From all these observations, the coupling could thus possibly be increased by further optimizing the thickness ratio of the heterostructure, or by exploiting a stronger magnetostrictive material like Terfenol [60–62].

As observed in Fig. 6(c), the coercive field trends as a function of the V_2O_3/CoFeB relative thickness decay much faster for thin CoFeB films rather than thick ones, independently on the V_2O_3 thicknesses. One must finally note that the interfacial coupling still affects the coercive field even for 30-nm-thick CoFeB on V_2O_3 (thicker than 25 nm).

IV. CONCLUSION

We tailored ferromagnetic heterostructures between amorphous CoFeB thin films and epitaxially grown V_2O_3 thin films by playing with the absolute thicknesses and explored their magnetic properties in the temperature range that crosses the V_2O_3 SPT. The V_2O_3 SPT leads to interfacial strains to the CoFeB layers that induce very large H_C variations, up to 330% at LT in the case of 80-nm-thick V_2O_3 and 3-nm CoFeB. Since the interfacial strain is due to the structural V_2O_3 expansion across its SPT, its effect on the magnetic properties of the ferromagnetic overlayer can be optimized by proper choice of the parameters, notably the thicknesses of the interfacing layers, which may lead to advanced magnetic heterostructure engineering.

[1] C. Song, B. Cui, F. Li, X. Zhou, and F. Pan, Recent progress in voltage control of magnetism: Materials, mechanisms, and performance, Prog. Mater. Sci. **87**, 33 (2017).

[2] C. A. F. Vaz, J. Hoffman, Y. Segal, M. S. J. Marshall, J. W. Reiner, Z. Zhang, R. D. Grober, F. J. Walker, and C. H. Ahn, Control of magnetism in Pb($Zr_{0.2}Ti_{0.8}$)O_3/$La_{0.8}Sr_{0.2}MnO_3$ multiferroic heterostructures (invited), J. Appl. Phys. **109**, 07D905 (2011).

[3] S. Mangin, M. Gottwald, C.-H. Lambert, D. Steil, V. Uhlíř, L. Pang, M. Hehn, S. Alebrand, M. Cinchetti, G. Malinowski, Y. Fainman, M. Aeschlimann, and E. E. Fullerton, Engineered materials for all-optical helicity-dependent magnetic switching, Nat. Mater. **13**, 286 (2014).

[4] N. Kanda, T. Higuchi, H. Shimizu, K. Konishi, K. Yoshioka, and M. Kuwata-Gonokami, The vectorial control of magnetization by light, Nat. Commun. **2**, 362 (2011).

[5] I. S. Camara, J.-Y. Duquesne, A. Lemaître, C. Gourdon, and L. Thevenard, Field-Free Magnetization Switching by an Acoustic Wave, Phys. Rev. Appl. **11**, 014045 (2019).

[6] L. Thevenard, J.-Y. Duquesne, E. Peronne, H. J. von Bardeleben, H. Jaffres, S. Ruttala, J.-M. George, A. Lemaître, and C. Gourdon, Irreversible magnetization switching using surface acoustic waves, Phys. Rev. B **87**, 144402 (2013).

[7] L. Thevenard, I. S. Camara, S. Majrab, M. Bernard, P. Rovillain, A. Lemaître, C. Gourdon, and J.-Y. Duquesne, Precessional magnetization switching by a surface acoustic wave, Phys. Rev. B **93**, 134430 (2016).

[8] A. Manchon, J. Železný, I. M. Miron, T. Jungwirth, J. Sinova, A. Thiaville, K. Garello, and P. Gambardella, Current-induced spin-orbit torques in ferromagnetic and antiferromagnetic systems, Rev. Mod. Phys. **91**, 035004 (2019).

[9] Y. Li, K. W. Edmonds, X. Liu, H. Zheng, and K. Wang, Manipulation of magnetization by spin-orbit torque, Adv. Quantum Technol. **2**, 1800052 (2019).

[10] A. Brataas, A. D. Kent, and H. Ohno, Current-induced torques in magnetic materials, Nat. Mater. **11**, 372 (2012).

[11] G. Vinai, F. Motti, V. Bonanni, A. Y. Petrov, S. Benedetti, C. Rinaldi, M. Stella, D. Cassese, S. Prato, M. Cantoni, G. Rossi, G. Panaccione, and P. Torelli, Reversible modification of ferromagnetism through electrically controlled morphology, Adv. Electron. Mater. **5**, 1900150 (2019).

[12] V. Polewczyk, G. Vinai, F. Motti, S. Dal Zilio, P. Capaldo, M. Sygletou, S. Benedetti, G. Rossi, and P. Torelli, Original design of a patterned multiferroic heterostructure for electrical control of the magnetic shape anisotropy, J. Magn. Magn. Mater. **507**, 166816 (2020).

[13] F. Motti, G. Vinai, V. Bonanni, V. Polewczyk, P. Mantegazza, T. Forrest, F. Maccherozzi, S. Benedetti, C. Rinaldi, M. Cantoni, D. Cassese, S. Prato, S. S. Dhesi, G. Rossi, G. Panaccione, and P. Torelli, Interplay between morphology and magnetoelectric coupling in Fe/PMN-PT multiferroic heterostructures studied by microscopy techniques, Phys. Rev. Materials **4**, 114418 (2020).

[14] A. A. Bukharaev, A. K. Zvezdin, A. P. Pyatakov, and Y. K. Fetisov, Straintronics: A new trend in micro- and nanoelectronics and material science, Usp. Fiz. Nauk **188**, 1288 (2018).

[15] K. J. Choi, M. Biegalski, Y. L. Li, A. Sharan, J. Schubert, R. Uecker, P. Reiche, Y. B. Chen, X. Q. Pan, V. Gopalan, L.-Q. Chen, D. G. Schlom, and C. B. Eom, Enhancement of ferroelectricity in strained $BaTiO_3$ thin films, Science **306**, 1005 (2004).

[16] E. Bousquet, M. Dawber, N. Stucki, C. Lichtensteiger, P. Hermet, S. Gariglio, J.-M. Triscone, and P. Ghosez, Improper ferroelectricity in perovskite oxide artificial superlattices, Nature (London) **452**, 732 (2008).

[17] H. Guo, S. Dong, P. D. Rack, J. D. Budai, C. Beekman, Z. Gai, W. Siemons, C. M. Gonzalez, R. Timilsina, A. T. Wong, A. Herklotz, P. C. Snijders, E. Dagotto, and T. Z. Ward, Strain Doping: Reversible Single-Axis Control of a Complex Oxide Lattice via Helium Implantation, Phys. Rev. Lett. **114**, 256801 (2015).

[18] D. Meng, H. Guo, Z. Cui, C. Ma, J. Zhao, J. Lu, H. Xu, Z. Wang, X. Hu, Z. Fu, R. Peng, J. Guo, X. Zhai, G. J. Brown, R. Knize, and Y. Lu, Strain-induced high-temperature perovskite ferromagnetic insulator, Proc. Natl. Acad. Sci. USA **115**, 2873 (2018).

[19] K. Ahadi, L. Galletti, Y. Li, S. Salmani-Rezaie, W. Wu, and S. Stemmer, Enhancing superconductivity in $SrTiO_3$ films with strain, Sci. Adv. **5**, eaaw0120 (2019).

[20] D. Sander, R. Skomski, A. Enders, C. Schmidthals, D. Reuter, and J. Kirschner, The correlation between mechanical stress and magnetic properties of ultrathin films, J. Phys. D: Appl. Phys. **31**, 663 (1998).

[21] A. S. Melo, A. B. de Oliveira, C. Chesman, R. D. Della Pace, F. Bohn, and M. A. Correa, Anomalous nernst effect in stressed magnetostrictive film grown onto flexible substrate, Sci. Rep. **9**, 15338 (2019).

[22] I. K. Bdikin, J. Gracio, R. Ayouchi, R. Schwarz, and A. L. Kholkin, Local piezoelectric properties of ZnO thin films prepared by RF-plasma-assisted pulsed-laser deposition method, Nanotechnology **21**, 235703 (2010).

[23] V. Iurchuk, D. Schick, J. Bran, D. Colson, A. Forget, D. Halley, A. Koc, M. Reinhardt, C. Kwamen, N. A. Morley, M. Bargheer, M. Viret, R. Gumeniuk, G. Schmerber, B. Doudin, and B. Kundys, Optical Writing of Magnetic Properties by Remanent Photostriction, Phys. Rev. Lett. **117**, 107403 (2016).

[24] S. P. Bennett, A. T. Wong, A. Glavic, A. Herklotz, C. Urban, I. Valmianski, M. D. Biegalski, H. M. Christen, T. Z. Ward, and V. Lauter, Giant controllable magnetization changes induced by structural phase transitions in a metamagnetic artificial multiferroic, Sci. Rep. **6**, 22708 (2016).

[25] F. Motti, G. Vinai, A. Petrov, B. A. Davidson, B. Gobaut, A. Filippetti, G. Rossi, G. Panaccione, and P. Torelli, Strain-induced magnetization control in an oxide multiferroic heterostructure, Phys. Rev. B **97**, 094423 (2018).

[26] B. A. Frandsen, L. Liu, S. C. Cheung, Z. Guguchia, R. Khasanov, E. Morenzoni, T. J. S. Munsie, A. M. Hallas, M. N. Wilson, Y. Cai, G. M. Luke, B. Chen, W. Li, C. Jin, C. Ding, S. Guo, F. Ning, T. U. Ito, W. Higemoto, S. J. L. Billinge *et al.*, Volume-wise destruction of the antiferromagnetic mott insulating state through quantum tuning, Nat. Commun. **7**, 12519 (2016).

[27] A. S. McLeod, E. van Heumen, J. G. Ramirez, S. Wang, T. Saerbeck, S. Guenon, M. Goldflam, L. Anderegg, P. Kelly, A. Mueller, M. K. Liu, I. K. Schuller, and D. N. Basov, Nanotextured phase coexistence in the correlated insulator V_2O_3, Nat. Phys. **13**, 80 (2017).

[28] D. B. McWhan, A. Menth, J. P. Remeika, W. F. Brinkman, and T. M. Rice, Metal-insulator transitions in pure and doped V_2O_3, Phys. Rev. B **7**, 1920 (1973).

[29] G. Panaccione, M. Altarelli, A. Fondacaro, A. Georges, S. Huotari, P. Lacovig, A. Lichtenstein, P. Metcalf, G. Monaco, F. Offi, L. Paolasini, A. Poteryaev, M. Sacchi, and O. Tjernberg, Coherent Peaks and Minimal Probing Depth in Photoemission Spectroscopy of Mott-Hubbard Systems, Phys. Rev. Lett. **97**, 116401 (2006).

[30] J. Sakai, P. Limelette, and H. Funakubo, Transport properties and c/a ratio of V_2O_3 thin films grown on C- and R-plane sapphire substrates by pulsed laser deposition, Appl. Phys. Lett. **107**, 241901 (2015).

[31] E. B. Thorsteinsson, S. Shayestehaminzadeh, and U. B. Arnalds, Tuning metal-insulator transitions in epitaxial V_2O_3 thin films, Appl. Phys. Lett. **112**, 161902 (2018).

[32] B. Sass, C. Tusche, W. Felsch, N. Quaas, A. Weismann, and M. Wenderoth, Structural and electronic properties of epitaxial V_2O_3 thin films, J. Phys.: Condens. Matter **16**, 77 (2004).

[33] J. de la Venta, S. Wang, J. G. Ramirez, and I. K. Schuller, Control of magnetism across metal to insulator transitions, Appl. Phys. Lett. **102**, 122404 (2013).

[34] L. Dillemans, T. Smets, R. R. Lieten, M. Menghini, C.-Y. Su, and J.-P. Locquet, Evidence of the metal-insulator transition in ultrathin unstrained V_2O_3 thin films, Appl. Phys. Lett. **104**, 071902 (2014).

[35] Y. Kalcheim, C. Adda, P. Salev, M. Lee, N. Ghazikhanian, N. M. Vargas, J. del Valle, and I. K. Schuller, Structural manipulation of phase transitions by self-induced strain in geometrically confined thin films, Adv. Funct. Mater. **30**, 2005939 (2020).

[36] T. Saerbeck, J. de la Venta, S. Wang, J. G. Ramírez, M. Erekhinsky, I. Valmianski, and I. K. Schuller, Coupling of magnetism and structural phase transitions by interfacial strain, J. Mater. Res. **29**, 2353 (2014).

[37] Y. Kalcheim, N. Butakov, N. M. Vargas, M.-H. Lee, J. del Valle, J. Trastoy, P. Salev, J. Schuller, and I. K. Schuller, Robust Coupling Between Structural and Electronic Transitions in a Mott Material, Phys. Rev. Lett. **122**, 057601 (2019).

[38] D. A. Gilbert, J. G. Ramírez, T. Saerbeck, J. Trastoy, I. K. Schuller, K. Liu, and J. de la Venta, Growth-induced in-plane uniaxial anisotropy in V_2O_3/Ni films, Sci. Rep. **7**, 13471 (2017).

[39] C. Wang, C. Xu, M. Wang, Y. Yuan, H. Liu, L. Dillemans, P. Homm, M. Menghini, J.-P. Locquet, C. Van Haesendonck, S. Zhou, S. Ruan, and Y.-J. Zeng, Coupling of ferromagnetism and structural phase transition in V_2O_3/Co bilayers, J. Phys. D: Appl. Phys. **50**, 495002 (2017).

[40] B. Sass, S. Buschhorn, W. Felsch, D. Schmitz, and P. Imperia, Thin layers of Fe, Co and Ni on V_2O_3 and V_2O_3 (0001): A comparison of the interfacial magnetic interactions, J. Magn. Magn. Mater. **303**, 167 (2006).

[41] S. Ikeda, J. Hayakawa, Y. Ashizawa, Y. M. Lee, K. Miura, H. Hasegawa, M. Tsunoda, F. Matsukura, and H. Ohno, Tunnel magnetoresistance of 604% at 300 K by suppression of Ta diffusion in CoFeB/MgO/CoFeB pseudo-spin-valves annealed at high temperature, Appl. Phys. Lett. **93**, 082508 (2008).

[42] S. Ikeda, K. Miura, H. Yamamoto, K. Mizunuma, H. D. Gan, M. Endo, S. Kanai, J. Hayakawa, F. Matsukura, and H. Ohno, A perpendicular-anisotropy CoFeB–MgO magnetic tunnel junction, Nat. Mater. **9**, 721 (2010).

[43] T. Wada, T. Yamane, T. Seki, T. Nozaki, Y. Suzuki, H. Kubota, A. Fukushima, S. Yuasa, H. Maehara, Y. Nagamine, K. Tsunekawa, D. D. Djayaprawira, and N. Watanabe, Spin-transfer-torque-induced Rf oscillations in CoFeB/MgO/CoFeB magnetic tunnel junctions under a perpendicular magnetic field, Phys. Rev. B **81**, 104410 (2010).

[44] A. Ruiz-Calaforra, T. Brächer, V. Lauer, P. Pirro, B. Heinz, M. Geilen, A. V. Chumak, A. Conca, B. Leven, and B. Hillebrands, The role of the non-magnetic material in spin pumping and magnetization dynamics in NiFe and CoFeB multilayer systems, J. Appl. Phys. **117**, 163901 (2015).

[45] S. Cho, S. C. Baek, K.-D. Lee, Y. Jo, and B.-G. Park, Large spin hall magnetoresistance and its correlation to the spin-orbit torque in W/CoFeB/MgO structures, Sci. Rep. **5**, 14668 (2015).

[46] K. Wang, Z. Xu, Y. Huang, Y. Qiu, and S. Dong, Magnetic, thermal, electrical properties and crystallization kinetics of $Co_{60}Fe_{20}B_{20}$ alloy films, Sci. China Mater. **59**, 639 (2016).

[47] Y.-T. Chen and W. H. Hsieh, Thermal, magnetic, electric, and adhesive properties of amorphous $Co_{60}Fe_{20}B_{20}$ thin films, J. Alloys Compd. **552**, 283 (2013).

[48] G. Vinai, F. Motti, A. Y. Petrov, V. Polewczyk, V. Bonanni, R. Edla, B. Gobaut, J. Fujii, F. Suran, D. Benedetti, F. Salvador, A. Fondacaro, G. Rossi, G. Panaccione, B. A. Davidson, and P. Torelli, An integrated ultra-high vacuum apparatus for growth and in situ characterization of complex materials, Rev. Sci. Instrum. **91**, 085109 (2020).

[49] A. Moatti, R. Sachan, J. Prater, and J. Narayan, Control of structural and electrical transitions of VO_2 thin films, ACS Appl. Mater. Interfaces **9**, 24298 (2017).

[50] S. K. Chaluvadi, D. Mondal, C. Bigi, D. Knez, P. Rajak, R. Ciancio, J. Fujii, G. Panaccione, I. Vobornik, G. Rossi, and P. Orgiani, Pulsed laser deposition of thin films by means of Nd:YAG laser source operating at its 1st harmonic: Recent approaches and advances, J. Phys. Mater. (2021).

[51] N. Chowdhury and S. Bedanta, Controlling the anisotropy and domain structure with oblique deposition and substrate rotation, AIP Adv. **4**, 027104 (2014).

[52] L. W. Finger and R. M. Hazen, Crystal structure and isothermal compression of Fe_2O_3, Cr_2O_3, and V_2O_3 to 50 Kbars, J. Appl. Phys. **51**, 5362 (1980).

[53] L. Dillemans, R. R. Lieten, M. Menghini, T. Smets, J. W. Seo, and J.-P. Locquet, Correlation between strain and the metal–insulator transition in epitaxial V_2O_3 thin films grown by molecular beam epitaxy, Thin Solid Films **520**, 4730 (2012).

[54] J.-P. Maria, S. Trolier-McKinstry, D. G. Schlom, M. E. Hawley, and G. W. Brown, The influence of energetic bombardment on the structure and properties of epitaxial $SrRuO_3$ thin films grown by pulsed laser deposition, J. Appl. Phys. **83**, 4373 (1998).

[55] B. S. Allimi, M. Aindow, and S. P. Alpay, Thickness dependence of electronic phase transitions in epitaxial V_2O_3 films on (0001) $LiTaO_3$, Appl. Phys. Lett. **93**, 112109 (2008).

[56] A. Yamaguchi, T. Ohkochi, A. Yasui, T. Kinoshita, and K. Yamada, Heterojunction-induced magnetic anisotropy and magnetization reversal of Ni wires on $LiNbO_3$ substrate, J. Magn. Magn. Mater. **453**, 107 (2018).

[57] A. Mougin, C. Dufour, K. Dumesnil, N. Maloufi, and P. Mangin, $DyFe_2$ (110) nanostructures: Morphology and magnetic anisotropy, Appl. Phys. Lett. **76**, 1449 (2000).

[58] L. Kipgen, H. Fulara, M. Raju, and S. Chaudhary, In-plane magnetic anisotropy and coercive field dependence upon thickness of CoFeB, J. Magn. Magn. Mater. **324**, 3118 (2012).

[59] Y.-T. Chen and S. M. Xie, Magnetic and electric properties of amorphous $Co_{40}Fe_{40}B_{20}$ thin films, J. Nanomater. **2012**, 486284 (2012).

[60] A. E. Clark, Chapter 7 Magnetostrictive rare earth-Fe_2 Compounds, Handbook Ferromag. Mater. **1**, 531 (1980).

[61] V. Polewczyk, M. Hehn, A. Hillion, S. Robert, P. Boulet, and K. Dumesnil, Epitaxial growth of $TbFe_2$ on piezoelectric $LiNbO_3$ Z-cut, J. Phys.: Condens. Matter **32**, 235803 (2020).

[62] V. Polewczyk, M. Hehn, A. Hillion, S. Robert, P. Boulet, and K. Dumesnil, Epitaxial growth of magnetostrictive $TbFe_2$ films on piezoelectric $LiNbO_3$, J. Phys.: Condens. Matter **31**, 405801 (2019).